Melting in the Earth's Deep Interior

Guillaume Fiquet

Melting in the Earth's deep Interior

Guillaume Fiquet

Institut de Minéralogie, de Physique des Matériaux et de Cosmochimie - IMPMC
Sorbonne Université, UMR CNRS 7590
Muséum National d'Histoire Naturelle, IRD
4 Place Jussieu, 75005 Paris France

Keywords : partial melting, solidus, liquidus, deep Earth, Earth's mantle, ULVZ, melts, peridotite, MORB.

Abstract

In this article, I focus on melting in the deep Earth from the transition zone to the core mantle boundary, with a brief overview of recent works dedicated to such melting properties. Two regions in the deep Earth are likely to be the locus of partial melting of the mantle: the transition zone and the core mantle boundary. In the transition zone region, melts can be produced on the top of the transition zone or at the top of the lower mantle. In the lower mantle, estimates of the initial core-mantle boundary (CMB) temperature exceeds the melting temperature of the mantle, indicating extensive lower mantle melting in the early Earth, compatible with the formation of a deep magma ocean. It is likely some relics of this early magma ocean have been kept at the core mantle boundary. Most measurements or calculations of iron partitioning between bridgmanite and the silicate indicate that these partial melts are likely to be gravitationally stable at the CMB. Further studies are required to evaluate the influence of light incompatible species such as H_2O and CO_2 on melting at the CMB, as are precise mechanisms for transportation and delivery of volatiles to the very deep mantle.

Introduction

Planetary accretion and differentiation of terrestrial planets into a metallic core and a rocky mantle are intimately related to melting processes. For the early Earth, it is established that silicate melts played an important role in shaping the Earth's interior as we see it today. Impacts are important events throughout the whole Earth's formation history, associated with release of gravitational energy (e.g. Ricard et al. 2009). The giant impact invoked in the formation of the Moon has probably been able to melt a large amount if not the whole silicate Earth (e.g. Canup, 2012; Nakajima and Stevenson, 2014), thus resulting in a magma ocean (Abe, 1997). Estimates of the melting or crystallization temperature of the Earth's mantle are thus important parameters to understand the Earth's history and its present state. At present, seismic waves mostly tell us that the Earth's mantle is not molten. Rocks

indeed melt only in exceptional circumstances (e.g. McKenzie, 1985), at very specific locations (see MELT seismic team, 1998 for instance). Partial melting of mantle rocks result from an increase of temperature, or a pressure drop, or the introduction of volatiles species such as water or carbon, which lowers the melting points of silicates (e.g. Kushiro et al., 1968, Canil and Scarfe, 1990; Dasgupta et al. 2005, Falloon and Green, 1989; Hirschmann, 2006, Litasov and Ohtani, 2003). A very abundant literature is available about this topic and the reader is also invited to consult Wyllie and Ryabchikov (2000) or a recent review paper by Green (2015).

What does melting in the Earth's deep interior thus means? It is not the intention of this chapter to cover all melting processes taking place beneath ridges and plumes, which have been described by almost 60 years of literature (Green and Ringwood, 1967; Yoder and Tilley, 1962, Anderson and Sammis, 1970 and references herein). I will not describe the partial melting in the asthenosphere (e.g. Chantel et al. 2016) nor treat the partial melting or crystallization in the Earth's core but rather expose recent interests for deep melts related with the transition zone, and deep primordial (or present) melts within the Earth's mantle, which may originate from fractional crystallization of a thick magma ocean.

In order to generate (or to keep) a melt, a general principle has to be obeyed. If we assume for instance a peridotite composition for the Earth's mantle, the geothermal gradient has either to be above the peridotite solidus or the temperature of the peridotite solidus has to be lowered. In phase diagrams, mixtures of components melt at a lower temperature than the pure end-members, and addition of a third component reduces both the solidus and liquidus temperatures in a two components system. Volatile components, such as H_2O and CO_2, are good candidates that can be considered, particularly at subduction zones, which cause the solidus and liquidus temperatures to be lowered and result in partial melting. Note that fluids released from subducting oceanic crust at depths greater than 100 km are supercritical fluids rather than aqueous fluid and/or hydrous melts (Mibe et al., 2011).

In this article, I will focus on melting at much greater depth, from the transition zone to the core mantle boundary. Many authors, coupling experimental and theoretical approaches, encompassing realistic mantle compositions as well as end-members, have addressed such melting properties. In this chapter, I will try to give a brief overview of these works.

Do we have geophysical evidences for melting in the deep Earth?

Over the past 30 years there has been an increased interest in the Core Mantle Boundary (CMB) region of the Earth. In the last decade, a great deal of effort has been focused on this region with improved seismic analysis techniques and compilations of analyses that yield a variety of interesting features (Garnero et. al. 1993; Garnero and Helmberger, 1998; Wysession, 1996). Such studies show reductions in S and P wave velocities (from 1-3% at large scales up to 10% or more at smaller scales) as well as strong lateral and radial

variations in this region. With the seismic assessments that the mid-mantle (1000km < z < 2000km) itself is largely homogeneous in comparison, with the exception of the subduction zone penetration of oceanic plates, this discovery has broad implications for the role of this region on Earth processes, ranging from plate behavior to convective dynamics and plume generation. Improvements in tomography suggest that subducting lithospheric slabs have a signature in the velocity perturbation of the whole Earth's mantle, and that the CMB could also be the repository of oceanic slabs subducted all the way down through the lower mantle (*e.g.* van der Hilst et al. 1997). The dynamics of such model corresponds to whole mantle convection in which subducted oceanic crust, transformed into a dense assemblage, partially segregates to form a D" layer growing with time (Coltice and Ricard, 1999). Hotspots arise from this deep thermal boundary layer and tap, in variable proportions, material from both the residual deep mantle and D". Old fragments of oceanic lithosphere and refractory cumulates from the magma ocean could host at the base of the mantle most of the primordial He and Ne observed today in oceanic basalts (Albarède, 2008). Other works suggest that plumes root at the CMB and chemical variability in this region will then be expressed at the surface *via* lava emission (Hoffman, 1997). It is obvious that fractional melting and crystallization processes linked to the thermal state and evolution of the mantle will significantly affect the distribution of geochemical species in the Earth's interior.

Seismology studies have presented the basic observations of two large low-shear velocity provinces (LLSVP) under the African continent and in the pacific basin, as shown **Figure 4.1** (e.g. Helmberger et al. 2005; Garnero and McNamara, 2008, McNamara et al. 2010; Yu and Garnero, 2017). A consensus view exists that these slow regions (which are possibly up to 1000 km thick) exhibit an anomalously low shear velocity and increased bulk modulus but LLSVPs are not thought to be partially molten. Ultralow-velocity zones (ULVZs) have been extensively documented by short-period studies. ULVZs correspond to localized features at the core mantle boundary (CMB), with strong reductions in seismic velocities (in the range of 10 to 30 %) for both P- and S- waves (e.g. Wen and Helmberger, 1998; Garnero and Helmberger, 1998; Garnero et al. 1993), and it was proposed these zones are partially molten (Williams and Garnero, 1996). A critical observation is that these "partially molten" regions are not laterally continuous, and have a thickness ranging from a presumed few kilometers up to about 50 km in some regions. These observations, coupled with the observed shear wave splitting (orthogonal polarizations of the S wave into SV and SH components) in D", yield direct implications for strong chemical and thermal heterogeneities in this region and the subsequent implications for chemical reactions between mantle and core, CMB dynamics and heat transport. High-resolution waveform studies also find evidence that the ULVZ materials are denser than the surrounding mantle (Rost et al. 2006). Furthermore, geodynamical calculations suggest that only a dense partially molten mixture produces partial melt distributions that are compatible with seismic observations of ULVZs (Hernlund and Tackley, 2007). As mentioned by Labrosse et al. (2007), the survival of a layer of melt formed at the base of the mantle early in its history also depends on whether it was (and may be still is) gravitationally and chemically stable. If it is the case, consequences could

be important because such a layer would be an ideal candidate for an un-sampled geochemical reservoir hosting a variety of incompatible species. A very important question is thus posed about the densification of melts at high-pressure, as well as for a high Grüneisen parameter, which both help to stabilize melt at the base of the mantle. These questions will be treated elsewhere in this special volume (please refer to Chapter 16 by P. Asimow).

Another region of interest in the deep Earth for possible deep melts is the transition zone. There is now little doubt that the Earth's transition zone is the repository of large amount of volatiles elements. The first direct evidence has been given by Pearson et al. (2014) who show the terrestrial occurrence of a hydrous ringwoodite included in a diamond from Juína (Brazil). The water-rich nature of this inclusion, indicated by infrared absorption, is indeed clear evidence that the transition zone can be hydrous, with about 1 weight percent of water. Schmandt et al. (2014) further demonstrate that dehydration could cause melting in a vertically flowing mantle. High-pressure laboratory experiments indeed evidence that the transition of hydrous ringwoodite to bridgmanite and (Mg,Fe)O is able to produce intergranular melt. Concomitantly, detection of abrupt decreases in seismic velocity using P-to-S conversions recorded by a dense seismic array in North America, where downwelling mantle is inferred, is consistent with partial melt below 660 kilometers. As ringwoodite crystals are entrained from the transition zone to the lower mantle by convection, higher temperatures and higher pressures prompt the water contained inside to exsolve, thus triggering melting.

Another region of interest has also been identified above the 410-km discontinuity. This layer characterized by low seismic wave velocities has been identified regionally (Revenaugh and Sipkin, 1994; Vinnik and Farra, 2007). This low velocity layer shows poor lateral continuity and it has been proposed that partial melting induced by local effects, such as the dehydration of subducted crust or the dehydration of water-bearing silicates beneath continental platforms in association with mantle plumes could explain these features. Additional observations at a regional scale are also compatible with the presence of a deep-seated melt or fluid layer on top of the 410-km deep seismic discontinuity (Toffelmier and Tyburczy, 2007, Song et al., 2004). Tauzin et al. (2010) report seismic observations from a large number of seismic stations worldwide that indicate a thick, intermittent low-velocity layer is located near 350 km depth in the mantle. The low velocity layer is thus not strictly limited to regions associated with subduction or mantle plumes, and shows no affinity to a particular tectonic environment, thus pointing toward the presence of a global layer of partial melt above the 410-km discontinuity. Such observations are supported by the model presented in Bercovici and Karato (2003), which predicts that the low-velocity layer should extend globally, because the weaker water storage capacity of upper mantle minerals should induce partial melting of water-bearing silicates throughout this region.

Melting diagrams for the Earth's lower mantle

In order to understand the thermodynamics of silicate liquids deeper in the Earth, several approaches have been developed. Dynamic compression experiments can reach high pressures and high temperature, above those prevailing at the core mantle boundary. A first estimate of the mantle solidus is given by the shock experiments by Holland and Ahrens (1997) on $(Mg,Fe)_2SiO_4$, which places an upper bound for the solidus of the ferropericlase and bridgmanite assemblage at 4300±270 K and 130±3 GPa. With the studies of Mosenfelder et al. (2009) and Thomas et al. (2012), some further constraints have been put on the calculation of isentropes in a multicomponent system CaO-MgO-Al_2O_3-SiO_2-FeO at elevated temperatures and pressures. The thermodynamic calculations made after these shock measurements show that a whole mantle magma ocean would first crystallize in the mid-lower mantle or at the base of the mantle were it composed of either peridotite or simplified "chondrite" liquid, respectively. Furthermore, concerning the hypothesis of the partial melt to explain the occurrence and characteristics of ultra-low velocity zones, Thomas et al. (2012) report that none of these candidate liquids is dense enough to remain at the core mantle boundary on geologic timescales, but their model defines a compositional range of liquids that would be gravitationally stable. It is clear that extensive fractional crystallization of Mg-Pv would need to take place before a liquid could be sufficiently enriched in iron so as to be dense enough to remain at the CMB at geological timescales.

Another approach has been to develop theoretical calculations about silicate liquid properties. First principles molecular dynamics simulations (de Koker et al. 2013; Stixrude et al. 2005, Stixrude et al. 2009) have predicted the melting curve of $MgSiO_3$ bridgmanite end-member, which increases monotonically with increasing pressure to reach 5400±600 K at the CMB. As shown in **Figure 4.2**, the mantle solidus can subsequently be estimated from the theoretical $MgSiO_3$ melting line, assuming a freezing point depression varying linearly with increasing pressure from the value of 340 K determined experimentally at 25 GPa by Tronnes and Frost (2002). The solidus temperature can be then calculated throughout the mantle. Stixrude et al. (2009) propose a melting temperature of 4100 K at the base of the mantle. At lower pressure, the calculations show a reasonable agreement with a solidus of a pyrolite-like composition determined experimentally up to 60 GPa by Zerr et al. (1998).

Melting phase relations and partial melt compositions have also been studied under deep lower mantle conditions in several diamond-anvil cell studies. These experiments have been carried out on different samples thought to be good proxies for the Earth's mantle composition: a peridotite composition (Fiquet et al. 2010; Tateno et al. 2014), a chondritic composition (Andrault et al. 2011), and a pyrolitic composition (Nomura et al. 2014). These experiments were carried out over a range of lower mantle pressures between 35 and 180 GPa, using laser-heated diamond-anvil cells (DAC), some of them coupled with *in situ* synchrotron measurements. Fiquet et al. (2010) and Andrault et al. (2011) used the combination of different observations to detect and/or bracket melting with *in situ* x-ray

diffraction and the (i) appearance of diffuse scattering, (ii) loss of diffraction peaks, (iii) rapid recrystallization, and (iv) sharp discontinuity in the relationship between laser power and sample measured temperature. Additional constraints are proposed in Fiquet et al. (2010) with the study of recovered samples sections prepared with focused ion beam (FIB) with high-resolution transmission electronic microscopy. Nomura et al. (2014) measured temperatures and proposed solidus temperatures on the basis of textural and chemical characterizations of the recovered samples only, *i.e.* the observation of melt segregation for instance. With a shorter duration of laser heating (around 1s) and no temperature measurement, Tateno et al. (2014) concentrated on the melting phase relations and iron partitioning using high-resolution spatial examination of textures in recovered samples.

There is a good agreement of solidus temperatures between with 4180±150 K reported for peridotite by Fiquet et al. (2010) and 4150±150 K for a chondritic composition by Andrault et al. (2011). The presence of 400 ppm of water has been invoked as the main reason for the lower solidus temperature of pyrolite of 3750K±200 K reported by Nomura et al. (2014), whereas the starting material studied by Fiquet al. (2010) is a dry peridotite glass obtained with laser-levitation. Solidus and liquidus are shown in **Figure 4.3** along with previous isentrope calculations by De Koker and Stixrude (2009) and results from shock experiments by Mosenfelder et al. (2009). The study of Tateno et al. (2014) is not reported because this work has been focused on the composition of the partial melts and not on the quantitative determination of melting temperatures. The comparison with the initial temperature estimated at about 4500 K or more at the CMB at 4.5 Ga (e.g. Gomi et al., 2013, Nakagawa and Tackley, 2010) shows that liquid isentrope lies mostly in the partial melting domain, thus indicating that deep melting makes sense in the early Earth.

Partial melt compositions and melting/crystallization sequences.

If we consider a peridotitic composition, the mantle stable assemblage is made of three phases: bridgmanite, $CaSiO_3$ with perovskite structure and (Mg,Fe)O ferropericlase (see **Figure 4.4**). The mantle solidus is of course much less than that of the end-members considered for the mantle. It is well established that (Mg,Fe)O is the liquidus phase (or the first phase to crystallize) at pressures below 30 GPa (Hirose and Fei 2002; Tronnes and Frost 2002; Ito et al. 2004). Above 31 GPa, Ito et al. (2004) showed that the stable phase at the liquidus changes to brigmanite. Furthermore, Liebske and Frost (2012) demonstrated, in the system $MgSiO_3$-MgO, that the eutectic composition becomes more MgO-rich with increasing pressures. At higher pressure, brigdmanite has been shown to be the stable phase at the liquidus (Fiquet et al. 2010; Tateno et al. 2014). Both studies agree on the melting sequence with ferropericlase and Ca-perovskite melting early in the sequence. Fiquet et al. (2010) clearly show that the bridgmanite, and not the post-bridgmanite, is the phase stable at the liquidus because post-bridgmanite converts back to brigmanite in the vicinity of the liquidus temperature. Both studies indicate that the melts formed are depleted in SiO_2 and enriched

in FeO with increasing pressure. These results are consistent with the most recent self-consistent thermodynamic calculations by Boukare et al. (2015) in the MgO-FeO-SiO_2 system as far as the crystallization sequence and the composition of the melt are concerned. Differences are more important however when one compares the liquidus of Boukare et al. (2015) with the liquidus temperatures found in experiments, which vary a lot from one to another. Though, these calculations do not integrate highly refractory elements such as aluminum or calcium, which may explain the higher liquidus reported in Fiquet et al. (2010). On the contrary, these calculations cannot explain the low liquidus of Andrault et al. (2011). Note also that liquidus temperatures are difficult to measure in experiments since liquids produced with laser heating in diamond-anvil cell experiments migrate along the temperature and pressure gradient created by the laser, hence modifying the local composition of the sample. Andrault et al. (2017) stress that this behavior may yield to an overestimation of the liquidus temperature for a given chemical composition, due to the loss of the most fusible elements.

Most experimental studies report a Fe-rich melt co-existing with the liquidus phase. These melts are not eutectic melts but formed by different degrees of partial melting, which may to some extent explain the differences. Tateno et al. (2014) and Nomura et al. (2011) indeed report a Fe partitioning D_{Fe} between melt and solids calculated as $D_{Fe}=[Fe^{solid}]/[Fe^{melt}]$ that diminishes with increasing pressure to reach 0.05 whereas Andrault et al. [2012] observe a small iron enrichment of the liquid with a D_{Fe} of 0.5-0.6 over a wide pressure range in the lower mantle. The partitioning of iron between bridgmanite and the melt controls the buoyancy of such melts and a possible accumulation of dense melts in the deep mantle. Andrault et al. (2017), in an attempt to reconcile measurements having conflicting conclusions, concludes that sinking melts are restricted to low partial melting degrees and highest mantle pressures. Even if the exact nature of the partitioning of iron between solid and liquid phases in the lower mantle is not completely cleared, most experimental and thermodynamic approaches seem to indicate that iron will partition into the melt phase. It is thus likely that melting in the $MgSiO_3$-$FeSiO_3$ system will produce magmas that are denser than the residual solids. Thomas et al. (2012) also suggest that the melt became denser in a later stage of solidification whereas it was enriched in FeO, therefore supporting the theory of a deep basal magma ocean concomitant with the late accretion stage of the Earth. Further recent studies such as that of Petitgirard et al. (2015) focus on the density contrast between solid and liquid silicate phases, and conclude that melts are denser than the surrounding solid phases in the lowermost mantle. Nature and densification of melts are also explored in other chapters of this volume.

Melting of MORB at the core mantle boundary

Very complementary to the studies on peridotite or pyrolite, melting properties of the subducted oceanic lithosphere –the other likely component present in the D" layer- have

also been explored extensively. Schematically, the oceanic lithosphere consists of a basaltic crust and an underlying harzburgitic component. The latter is more refractory than fertile peridotite and it is probably unlikely that it melts at mantle depths. MORB is a good proxy of the basaltic oceanic crust bulk composition. As shown in Pradhan et al. (2015), with high Si, Al, Fe and Na content in MORB, the mineral phases stable at lower mantle pressures are Mg- and Ca-perovskite (bridgmanite and CaPv), $CaFe_2O_4$-type (CF) phase and SiO_2 (St) - see **Figure 4.5**. At all pressures except between 13 to 18 GPa, a large number of studies showed that the anhydrous melting temperature of basaltic composition is lower than that of peridotitic mantle composition (Herzberg and Zhang 1996, Hirose et al. 1999, Zerr et al. 1998). At higher pressure, the study by Hirose et al. (1999) was the first one to suggest that MORB could possibly melt near the CMB. More recently, melting properties have been examined at CMB pressure and temperature conditions. Andrault et al. (2014) and Pradhan et al. (2015) used laser-heated diamond anvil cell (LHDAC) experiments. Results are reported in **Figure 4.6**. Both studies yield solidus temperatures at the CMB in agreement within error bars with 3800±150 K for Andrault et al. (2014) and 3970±150 K for Pradhan et al. (2015). At lower pressure, the latter is in very good agreement with previous diamond-anvil cell and multi-anvil results (Hirose et al. 1999; Hirose and Fei 2002). MORB is thus found to be slightly more fusible than peridotite. In Pradhan et al. (2015), the texture analysis allowed the authors to propose the following melting sequence (MgPv $\rightarrow SiO_2 \rightarrow$CaPv), which is identical to that reported from multi-anvil experiments by Hirose and Fei (2002). In Pradhan et al. (2015), chemical analyses of recovered samples at high spatial resolution using analytical transmission electron microscopy (TEM) also show that the quenched last melt is enriched in iron, which suggests that melt pockets may be gravitationally stable at the core mantle boundary. This result is very different from what has been reported by Andrault et al. (2014), which shows an increasing SiO_2 content in the liquid with increasing pressure, and the authors propose that SiO_2 reacts with the surrounding mantle to form brigdmanite. There are however some differences in the experimental procedures and in the analytical techniques between these two studies that may explain such different conclusions.

Influence of volatile incompatible elements

It is obvious that the volatile elements content of the deep mantle plays here a major role. Several hydrous mineral phases have been studied and proved to be stable at deep mantle conditions (Nishi et al. 2014; Ohtani et al. 2014; Ohira et al. 2014), thus opening up possibilities of deep-water transport. The H_2O storage capacity of the lower mantle is however uncertain and the subject of an ongoing controversy [Hirschmann, 2006; Ohtani, 2016 and references herein]. In the lower mantle, δ-AlOOH or phase H are unique hydrous minerals that could for instance supply water to the core mantle boundary and trigger dehydration melting (Ohtani, 2016). Garnero et al. (2016) note that the release of water in the lowermost mantle could indeed facilitate partial melting in thermochemical piles and further concludes that the incorporated basalt may undergo partial melting and react with

the pile material if piles have sufficiently high temperature (~3,500 K). If we attribute the low temperature solidus by Nomura et al. (2014) to the sole presence of 400 ppm H_2O, note that the melting depression is of the order of 500 K at the CMB. But at present, there are no real quantitative constraints on the amount of water transported, and may be released, in the lowermost mantle.

In the transition zone, melting is likely to occur with the help of incompatible species such as water. In the aforementioned transition-zone water-filter model proposed by Bercovici and Karato (2003), the melt thought to be denser than upper mantle minerals and lighter than transition zone minerals could be trapped above the 410-km discontinuity, which may be a reasonable model according to the observations by Tauzin et al. (2010). Similarly, the experimental investigation of the density of hydrous basaltic melt under pressure by Sakamaki et al. (2006) supports the idea that a low-velocity and high-attenuation region just above the mantle transition zone may result from the presence of a melt. The consequences of H_2O storage in the transition zone and the dehydration melting at the top of the lower mantle are also illustrated by the high-pressure laboratory experiments and the seismic observations by Schmandt et al. (2014).

Similarly, carbon is known to play a role in mantle melting. Partial melting and extraction of carbonatitic melts can be triggered by carbon dioxide down to depths of 300 km (Dasgupta and Hirschmann, 2006). A review of experiments focused on melting in the mantle in the presence of carbon is also given by Hammouda and Keshav (2015). The reader can also refer to Chapter 2 by Litasov. In the deep Earth, carbon is thought not only to induce melting but could also mobilize structurally bound mineral water (Dasgupta and Hirschmann, 2010). In the lowermost mantle however, very few is known about the transportation of carbon. Unlike water, which is in most of the Earth's mantle held in nominally anhydrous silicates, carbon is stored in accessory phases such as carbonates, diamond or alloys because of its very low solubility in deep Earth's minerals (Shcheka et al., 2006). High-pressure polymorphs of carbonates have been predicted to be stable at lower mantle conditions (Oganov et al. 2008) and then observed in experiments (Boulard et al. 2011; Merlini et al. 2015). Such phases could easily feed the core mantle boundary in carbon. But at present, a quantitative estimate of carbon or CO_2 release at the CMB remains unconstrained, as are precise mechanisms for transportation of volatiles to the very deep mantle.

Melting in the mantle and the thermal profile of the Earth

The fact that the core-mantle boundary is a thermal boundary layer is not questionable (e.g. Knittle and Jeanloz, 1991). Core temperatures are likely to be in excess of 4000 K at the CMB and the thermal state at the base of the mantle is tied to the temperature in the Earth's core and the heat flux through the CMB. Temperature of the Earth's core is anchored at the inner core – outer boundary and a function of the crystallization of the inner core crystallizing chemical system. Almost pure iron solidifies there to form the solid inner core and light

elements such as silicon, oxygen, sulfur, carbon or hydrogen are released in the liquid outer core (e.g. Poirier, 1994; Badro et al. 2007), thus providing an additional gravitational energy contributing to fuel the geodynamo. Temperatures at the CMB probably lay between 4300 and 3500 K, depending of the melting point depression created by the light elements content of the core (see **Figure 4.7**). As shown in this figure, the solidus temperatures of most of these systems at the CMB are of the order of the temperatures estimated for the CMB (depicted here as a green circle). The possibility for a melt to be preserved at the core-mantle boundary, at least in pockets, is thus high. Incompatible elements such as H_2O or CO_2 may help and trigger melting if dehydration or CO_2 is released at the CMB, even if no quantitative estimates of the delivery of these compounds at the CMB are clearly established at present. Note that the melt region defined with the wet solidus by Nomura et al. (2014) lies well below the temperature estimates at the CMB shown in Figure 4.7.

Conclusions

Two regions in the deep Earth are likely to be the locus of partial melting of the mantle: the transition zone and the core mantle boundary. In the transition zone region, melts can be produced on the top of the transition zone or at the top of the lower mantle. These melts will be produced by dehydration of the high-pressure polymorphs of olivine, which are important host for water at these depths. A wet transition zone is now a hypothesis that became a reality with the work of Pearson et al. (2014), though one inclusion in a diamond from one specific location is no proof of ubiquity. Recent experimental work and seismic studies however tend to show that low velocity regions compatible with the existence of a melt can be observed in very general geological settings at 410 and 670 km depths (Song et al., 2004, Tauzin et al. 2015, Schmandt et al., 2014).

Estimates of the initial CMB temperature exceed the melting temperature of the mantle, indicating extensive lower mantle melting in the early Earth leading to the formation of a deep magma ocean. If the evolution of a terrestrial magma ocean resulted in the formation of a layer of melt at the base of the mantle early in Earth history, it is likely some relics of this early magma ocean have been kept at the core mantle boundary. It is not completely clear where the crystallization of such a magma ocean could start, since both liquidus and isentrope depend on composition (Thomas et al., 2012). A global melting at the CMB also seems questionable. As noted by Hernlund and Tackley (2007), the partial melting of ordinary mantle should introduce a ubiquitous partially molten layer above an isothermal core–mantle boundary as a consequence of its isothermal and isobaric conditions. We can however envisage variations in thickness, with the thickest portions occurring at the base of upwelling plumes and a thin layer elsewhere, that may not be detected since seismology is possibly blind to thicknesses less than 5 km at the CMB. Even if mantle-melting temperatures remains uncertain due to differences in experimental methodologies in existing studies, the hypothesis of the presence of a deep magma ocean on the top of the Earth's core, which could be as thick as 50 km and explain the presence of ULVZs shown by seismology, is reasonable. Though it is still a matter of discussion, the liquids produced

during partial melting are dense and can hold multiple chemical elements, among which are important markers of the dynamics of the Earth's mantle. Such a layer would thus be an ideal candidate for an un-sampled geochemical reservoir hosting a variety of incompatible species, notably the planet's missing budget of heat-producing elements.

The solidus curve of MORB appears to be slightly lower than the temperature profile in the D" region estimated from melting of Fe at ICB conditions (Anzellini et al. 2013). If these temperatures at CMB were to be confirmed, it appears likely that the ULVZ could be partly made of dense partially melted MORB as well as partial melts formed in peridotite. Without considering the effects of possible re-equilibration of the partial melt, measurements of iron partitioning between Mg-bridgmanite and the silicate melt and preliminary analysis based on the model provided by Funamori and Sato (2010) indicate that these partial melts are likely to be gravitationally stable at the CMB.

Further studies are however required to confirm if such partial melts are indeed truly enriched in FeO and can be stabilized at the CMB or if melt pockets will just be swept by mantle circulation and recrystallize or react with the surrounding materials along their way back up in hot plumes or at the edge of chemical piles. The influence of light incompatible elements such as H_2O and CO_2 on melting at the core mantle boundary will also have to be ascertained, as are precise mechanisms for transportation and delivery of volatiles to the very deep mantle.

Acknowledgments

I warmly thank Shule Yu and Ed Garnero for the preparation and the communication of the Figure 4.1 before publication. I also acknowledge Denis Andrault for the figure 4.7 that has been modified from one of his earlier work. I also thank H. Bureau for a careful reading of the initial manuscript.

References

Abe, Y., 1997. Thermal and chemical evolution of the terrestrial magma ocean. Phys. Earth Planet. Int. 100, 27-39.

Albarede, F., 2008. Rogue mantle helium and neon. Science, 319 :943-945.

Anderson D. L., Spetzler H., 1970. Partial melting and the low-velocity zone. Phys. Earth Planet. Inter. 4, 62–64.

Anderson D.L., Sammis, C., 1970. Partial melting in the upper mantle. Phys. Earth Planetary Int. 3, 41, 50.

Andrault, D., Bolfan-Casanova, N., Bouhifd, M.A., Boujibar, A., Garbarino, G., Manthilake, G. Mezouar, M., Monteux, J., Parisiadis, P., Pesce, G., 2017. Toward a coherent model for the melting behavioir of the deep Earth's mantle. Phys. Earth Planet. Int. 265, 67-81.

Andrault, D., Bolfan-Casanova, N., Lo Nigro, G., Bouhifd, M.A., Garbarino, G., Mezouar, M., 2011. Melting curve of the deep mantle applied to properties of early magma ocean and actual core-mantle boundary. Earth Planet. Sci. Lett. 304, 251-259.

Andrault, D., Monteux, J., Le Bars, M., Samuel, H. 2016. The deep Earth may not be cooling down. Earth Planet. Sci. Lett. 443, 195-203.

Andrault, D., Pesce, G., Bouhifd, M.A., Bolfan-Casanova, N., Hénot, J.M., Mezouar, M., 2014. Melting of subducted basalt at the core-mantle boundary. Science 344 (6186) 892-895.

Anzellini, S., Dewaele, A., Mezouar, M., Loubeyre, P., Morard, G., 2013. Melting of Iron at Earth's Inner Core Boundary Based on Fast X-ray diffraction. Science 340, 464-466, doi:10.1126/science.1233514.

Badro, J., Fiquet, G., Guyot, F., Gregoryanz, E., Occelli, F., Antonangeli, D., d'Astuto, M., 2007. Effect of light elements on the sound velocities in solid iron: Implications for the composition of Earth's core. Earth Planet. Sci. Lett. 254, 233–238.

Bercovici, D., Karato, S., 2003. Whole mantle convection and transition-zone water filter. Nature 425, 39–44.

Boukare, C.E., Ricard, Y., Fiquet, G., 2015. Thermodynamics of the MgO-FeO-SiO_2 system up to 140 GPa: Application to the crystallization of Earth'smagma oceanJ. Geophys. Res. Solid Earth 120, 6085–6101, doi:10.1002/2015JB011929.

Boulard, E., Gloter, A., Corgne, A., Antonangeli, D., Auzende, A-L., Perrillat, J.P., Guyot, F., Fiquet, G., 2011. New host for carbon in the deep Earth. Proc. Nat. Acad. Sci. of America, doi/10.1073/pnas.1016934108.

Brown, J.M., Shankland, T.S., 1981. Thermodynamic parameters in the Earth as determined from seismic profiles. J. R. Astron. Soc. 66, 579.

Bunge, H.P., Ricard, Y., Matas, J., 2001. Non adiabaticity in mantle convection. Geophys. Res. Lett. 28, 879-882.

Canil, D., Scarfe, C. M., 1990. Phase relations in peridotite + CO_2 systems to 12 GPa: implications for the origin of kimberlite and carbonate stability in the Earth's upper mantle. J. Geophys. Res. 95, 15805–15816.

Canup, R.M., 2012. Forming a Moon with an Earth-like composition via a giant impact. Science 338 (6110) 1052-1055, doi:10.1126/science.1226073.

Chantel, J., Manthilake, G., Andrault, D., Novella, D., Yu, T., Wang, Y., 2016. Experimental evidence supports mantle partial melting in the astenosphere. Science Advances (2) 5, e1600246, doi:10.1126/sciadv. 1600246.

Christensen, U.R, Hofmann, A.W., 1994. Segregation of subducted oceanic crust in the convecting mantle. J. Geophys. Res. 99 (19), 867-884.

Coltice, N., Ricard, Y., 1999. Geochemical observations and one layer mantle convection. Earth Planet. Sci. Lett. 174, 125-137.

Dasgupta, R., Hirschmann, M. M., Dellas, N., 2005. The effect of bulk composition on the solidus of carbonated eclogite from partial melting experiments at 3 GPa. Contrib. Mineral. Petrol. 149, 288–305.

Dasgupta, R., Hirschmann, M.M., 2010. The deep carbon cycle and melting in Earth’s interior. Earth Planet. Sci. Lett. 298 (1-2) 1-13.

de Koker, N., Karki, B.B., Stixrude, L., 2013. Thermodynamics of the MgO–SiO2 liquid system in Earth’s lowermost mantle from first principles. Earth Planet. Sci. Lett. 361, 58–63.

Falloon, T. J., Green, D.H., 1989. The solidus of carbonated fertile peridotite. Earth Planet. Sci. Lett. 94, 364–370.

Fiquet, G., Auzende, A.L., Siebert, J., Corgne, A., Bureau, H., Ozawa, H., Garbarino, G. 2010. Melting of peridotite to 140 GPa. Science 329, 1516-1518.

Funamori, N., Sato, T., 2010. Density contrast between silicate melts and crystals in the deep mantle: An integrated view based on static compression data. Earth Planet. Sci. Lett., 295, 435–440, doi:10.1016/j.epsl.2010.04.021.

Garnero, E.J., Grand, S.P., Helmberger, D.V., 1993. Low P-wave velocity at the base of the mantle. Geophysical Research Letters 20, 1843-1846.

Garnero, E.J., Helmberger, D.V., 1998. Further structural constraints and uncertainties of a thin laterally varying ultralow-velocity layer at the base of the mantle. Journal of Geophysical Research – Solid Earth 103, 12495-12509.

Garnero, E.J., Lay, T., 1998. Effects of D'' anisotropy on seismic velocity models of the outermost core. Geophysical Research Letters 25, 2341-2344.

Garnero, E.J., McNamara, A.K., 2008. Structure and Dynamics of Earth's Lower Mantle. Science 320, 5876, 626-628.

Garnero, E.J., McNamara, A.K., Shim, S-H., 2016. Continent-sized anomalous zones with low seismic velocity at the base of Earth's mantle. Nature geoscience, doi: 10.1038/NGEO2733.

Gomi, H., Ohta, K., Hirose, K., Labrosse, S., Caracas, R., Verstraete, M.J., Hernlund J.W., 2013. The high conductivity of iron and thermal evolution of the Earth's core. Phys. Earth Planet. Int. 224, 88-103.

Green, D.H., Ringwood, A.E., 1967. The genesis of basaltic magmas. Contr. Mineral. and Petrol., 15, 103–190.

Green, D.H., 2015. Experimental petrology of peridotites, including effects of water and carbon on melting in the Earth's upper mantle. Phys. Chem. Minerals, doi : 10.1007/s00269-014-0729-2

Gu, Y.J., Lerner-Lam, A.L., Dziewonski, A.M., Ekstrom, G., 2005. Deep structure and seismic anisotropy beneath the East Pacific Rise. Earth Planet. Sci. Lett. 232, 259–272.

Hammouda, T., Keshav, S. 2015. Melting in the mantle in the presence of carbon: Review of experiments and discussion on the origin of carbonatites. Chem. Geol. 418, 171-188.

Helmberger, D., Lay, T., Ni, S., Gurnis, M., 2005. Deep mantle structure and the post-perovskite phase transition. Proc Natl Acad Sci U S A. 2005 November 29; 102(48) 17257–17263.

Hernlund, J.W., Labrosse, S., 2007. Geophysically consistent values of the perovskite to post-perovskite transition Clapeyron slope. Geophys. Res. Lett., 34, L05309, doi:10.1029/2006GL028961, 2007

Hernlund, J.W., Tackley, P.J., 2007. Some dynamical consequences of partial melting in earth's deep mantle. Physics of the Earth and Planetary Interiors 162, 149-163.

Hernlund, J.W., Thomas, C., Tackley, P.J., 2005. A doubling of the post-perovskite phase boundary and structure of the Earth's lowermost mantle. Nature 434, 882-886.

Herzberg, C., Zhang, J., 1996. Melting experiments on anhydrous peridotite KLB-I: Compositions of magmas in the upper mantle and transition zone. J. Geophys.Res. 101, B4, 8271-8295.

Hirose, K, Fei, Y.W., Ma, Y.Z., Mao, H.K. 1999. The fate of subducted basaltic crust in the Earth's lower mantle. Nature 397, 53-56.

Hirose, K., Fei, Y.W., 2002. Subsolidus and melting phase relations of basaltic composition in the uppermost lower mantle. Geochimi. Cosmochim. Acta 66, 2099-2108.

Hirschmann, M.M., 2006. Water, melting, and the deep Earth H_2O cycle. Annu Rev Earth Planet Sci. 34, 629–653.

Hofmann, A.W., 1997. Mantle geochemistry: the message from oceanic volcanism. Nature 385, 219 – 229, doi:10.1038/385219a0.

Holland, K.G, Ahrens, T.J. 1997. Melting of (Mg,Fe)2SiO4 at the core-mantle boundary of the Earth. Science 275, 1623-1625.

Ito, E., Kubo, A., Katsura, T., Walter, M.J., 2004. Melting experiments of mantle materials under lower mantle conditions with implications for magma ocean differentiation. Physics of the Earth and Planetary Interiors 143–144, 397–406.

Kato, T., Ringwood, A.E., Irifune, T., 1988. Experimental determination of element partitioning between silicate perovskites, garnets and liquids – constraints on early differenciation of the mantle. Earth and Planetary Science Letters 89: 123-145.

Katsura, T., Yoneda, A., Yamazaki, D., Yoshino, T., Ito, E., 2010. Adiabatic temperature profile in the mantle. Phys. Earth Planet. Int. 183, 212-218.

Knittle, E., Jeanloz, R., 1991. Earth's core-mantle boundary: results of experiments at high pressures and temperatures. Science 251, 1438-1443.

Kushiro, I., Syono, Y., Akimoto, S-I., 1968. Melting of a peridotite nodule at high pressures and high water pressures. J. Geophys. Res. 73 (18) 6023-6029.

Labrosse, S., Hernlund, J.W., Coltice, N., 2007. A crystallizing dense magma ocean at the base of the Earth's mantle. Nature 450, 866-869, doi:10.1038/nature06355.

Labrosse, S., Hernlund, J.W., Hirose, K., 2015. Fractional melting and freezing in the deep mantle and implications for the formation of a basal magma ocean. In, Badro, J., Walter, M.J. (Eds), The early Earth: Accretion and differentiation, Geophysical Monograph 212, 123-142.

Liebske, C., Frost, D.J., 2012. Melting phase relations in the MgO-MgSiO3 system between 16 and 26 GPa: Implications for melting in Earth's deep interior. Earth Planet. Sci. Lett. 345, 159-170.

Litasov, K.D., Ohtani, E., 2003. Phase relations and melt compositions in CMAS pyrolite-H_2O system up to 25 GPa. Phys. Earth Planet. Int. 134, 105-127.

Matas, J., Bass, J.D., Ricard, Y. et al., 2007. On the bulk composition of the lower mantle: predictions and limitations from generalized inversion of radial seismic profiles. Geophysical Journal International 170, 764-780

McKenzie, D., 1985. The extraction of magma from the crust and mantle. Earth Planet. Sci. Lett. 74, 81–91.

McNamara, A., Garnero,E.J., Rost, S., 2010. Tracking deep mantle reservoirs with ultra-low velocity zones. Earth and Planetary Science Letters 299, 1–9.

MELT Seismic Team, 1998. Imaging the deep seismic structure beneath a mid-ocean ridge: the MELT experiment. Science 280, 1215–1218.

Merlini, M., Hanfland, M., Salamat, A., Petitgirard, S., Müller, H., 2015. The crystal structures of $Mg_2Fe_2C_4O_{13}$, with tetrahedrally coordinated carbon, and $Fe_{13}O_{19}$, synthesized at deep mantle conditions. American Mineralogist 100, 2001-2004.

Mibe, K., Kawamoto, T., Matsukage, K.N., Fei, Y., Ono, S., 2011. Slab melting versus slab dehydration in subduction-zone magmatism. Proc. Nat. Acad. Sci. of America 108 (20) 8177-8182, doi/10.1073/pnas.1010968108 .

Morard, G., Andrault, D., Antonangeli, D., Bouchet, J., 2014. Properties of iron alloys under Earth's core conditions. C.R. Geoscience 346, 130-139.

Mosenfelder, J.L., Asimow, P.D., Ahrens, T.J., 2007. Thermodynamic properties of Mg_2SiO_4 liquid at ultra-high pressures from shock measurements to 200 GPa on forsterite and wadsleyite. Journal of geophysical research – Solid Earth 112, B06208.

Mosenfelder, J.L., Asimow, P.D., Frost, D.J., Rubie, D.C., Ahrens, T.J., 2009. The $MgSiO_3$ system at high pressure: Thermodynamic properties of perovskite, post-perovskite, and melt from global inversion of shock and static compression data. J. Geophys. Res. 114, B01203.

Nakagawa, T., and P. J. Tackley (2010), Influence of initial CMB temperature and other parameters on the thermal evolution of Earth's core resulting from thermochemical spherical mantle convection, Geochem. Geophys. Geosyst., 11, Q06001, doi:10.1029/2010GC003031.

Nakajima, M., Stevenson, D.J., 2014. Investigation of the initial state of the moon-forming disk: Bridging SPH simulations and hydrostatic models. Icarus 233, 259-267, doi:10.1016/j.icarus.2014.01.008.

Nimmo, F., Price, G.D., Brodholt, J., Gubbins, D., 2004. The influence of potassium on core and geodynamo evolution. Geophys. J. Int. 156, 363-376.

Nishi, M. et al., 2014. Stability of hydrous silicate at high pressures and water transport to the deep lower mantle. Nature Geosci. 7**,** 224–227.

Oganov, A.R., Ono, S., 2004. Theoretical and experimental evidence for a post-perovskite phase of MgSiO3 in Earth's D" layer. Nature 430, doi:10.1038/nature02701.

Oganov, A.R., Ono, S., Ma, Y., Glass, C.W., Garcia, A. 2008. Novel high-pressure structures of $MgCO_3$, $CaCO_3$, and CO_2 and their role in Earth's lower mantle. Earth Planet. Sci. Lett. 273, 38–47.

Ohira, I. et al., 2014. Stability of a hydrous δ-phase, AlOOH-$MgSiO_2(OH)_2$, and a mechanism for water transport into the base of lower mantle. Earth Planet. Sci. Lett. 401**,** 21–27.

Ohtani, E., Amaike, Y., Kamada, S., Sakamaki, T., Hirao, N., 2014. Stability of hydrous phase H $MgSiO_4H_2$ under lower mantle conditions. Geophys. Res. Lett. 41**,** 8283–8287.

Pearson, D.G., Brenker, F.E., Nestola, F., McNeill, J., Nasdala, L., Hutchison, M.T., Matveev, S., Mather, K., Silversmit, G., Schmitz, S., Vekemans, B., Vincze, L., 2014. Hydrous mantle transition zone indicated by ringwoodite included within diamond. Nature 507 (7491), 221, doi:10.1038/ nature13080.

Petitgirard, S., Malfait, W.J., Ryosuke, S., Kupenkova, I., Hennet, L., Harriese, D., Danec, T., Burghammer, T., Rubie, D.C., 2015. Fate of $MgSiO_3$ melts at core–mantle boundary

conditions. Proc. Nat. Acad. Sci. of America, 112 (46) 14186–14190, doi/10.1073/pnas.1512386112

Poirier, J.P., 1994. Light elements in the Earth's outer core: A critical review. Phys. Earth Planet. Int. 85, 319-337.

Pradhan, G.K., Fiquet, G., Siebert, J., Auzende, A.L., Morard, G., Antonangeli, D., Garbarino, G., 2015. Melting of MORB at core-mantle boundary. Earth Planet. Sci. Lett. 431, 247-255.

Presnall, D.C, Weng, Y.H., Milholland, C.S. et al., 1998. Liquidus phase relations in the system MgO-$MgSiO_3$ at pressures up to 25 GPa - constraints on crystallization of a molten Hadean mantle. Physics of the earth and Planetary Interiors 107 (1-3) 83-95.

Revenaugh, J., Sipkin, S., 1994. Seismic evidence for silicate melt atop the 410-km discontinuity. Nature 369, 474–476.

Ricard, Y., Šràmek, O., Dubuffet, F., 2009. A multi-phase model of runaway core-mantle segregation in planetary embryos. Earth Planet. Sci. Lett. 284 (1-2) 144-150, doi:10.1016/j.epsl.2009.04.021.

Ritsema, J., Deuss, A., Van Heijst, H.J., Woodhouse, J.H., 2011. S40RTS: a degree-40 shear-velocity model for the mantle from new Rayleigh wave dispersion, teleseismic traveltime and normal-mode splitting function measurements. Geophysical Journal International 184 (3) 1223–1236.

Rost, S., Garnero, E.J., Williams, Q., 2006. Fine-scale ultralow-velocity zone structure from high-frequency seismic array data. Journal of Geophysical Research – solid Earth 111, B09310.

Sakamaki, T., Suzuki, A., Ohtani, E., 2006. Stability of hydrous melt at the base of the Earth's upper mantle. Nature 439, 192-194, doi:10.1038/nature04352.

Schmandt, B., Jacobsen, S.D., Becker, T.W., Liu, Z., Dueker, K.D., 2014. Dehydration melting at the top of the lower mantle. Science 344, 1265, doi:10.1126/science.1253358.

Shcheka, S.S., Wiedenbeck, M., Frost, D.J., Keppler, H., 2006. Carbon solubility in mantle minerals. Earth Planet Sci Lett 245, 730–742.

Simon, F., Glatzel, G., 1929. Remarks on fusion pressure curve. Z. Anorg. Allg. Chem.178, 309–316, doi.org/10.1002/zaac.19291780123.

Song, T-R., Helmberger, D.V, Grand, S.P., 2004. Low-velocity zone atop the 410-km seismic discontinuity in the northwestern United States. Nature 427, 530-533.

Steinle-Neumann, G., Stixrude, L., Cohen, R. E., Gulseren, O., 2001. Elasticity of iron at the temperature of the Earth' s inner core. Nature 413, 57-60.

Stixrude, L., de Koker, N., Sun, N., Mookherjee, M., Karki, B.B., 2009. Thermodynamics of silicate liquids in the deep Earth. Earth and Planetary Science Letters 278, 226-232.

Stixrude, L., Karki, B., 2005. Structure and freezing of $MgSiO_3$ liquid in the Earth's lower mantle. Science 310, 5746, 297-299.

Tarduno, J.A., Cottrell, R.D., Watkeys, M.K., Bauch, D., 2007. Geomagnetic field strength 3.2 billions years ago recorded by single silicate crystals. Nature 446, 7136, 657-660.

Tateno, S., Hirose, K., Ohishi, Y., 2014. Melting experiments on peridotite to lowermost mantle conditions. J. Geophys. Res. Solid Earth 119, 4684-4694, doi:10.1002/2013JB010616.

Tauzin, B., Debayle, E., Wittlinger, G. 2010. Seismic evidence for a global low-velocity layer within the Earth's upper mantle. Nature geosciences 3, 718-721, doi:10.1038/ngeo969.

Thomas, C.W., Liu, Q., Agee, C.B., Asimow, P.D., Lange, R.A., 2012. Multi-technique equation of state for Fe2SiO4 melt and the density of Fe-bearing silicate melts form 0 to 161 GPa. J. Geophys. Res. 117, B10206, doi:10.1029/2012JB009403.

Toffelmier, D.A., Tyburczy, J.A., 2007. Electromagnetic detection of a 410-km-deep melt layer in the southwestern United States. Nature 447, 991-994, doi:10.1038/nature05922.

Trønnes, R.G., Frost, D.J., 2002. Peridotite melting and mineral-melt partitioning of major and minor elements at 22-24.5 GPa. Earth Planet. Sci. Lett. 197 (1-2), 117-131.

Tsuchiya, J., 2013. First principles prediction of a new high-pressure phase of dense hydrous magnesium silicates in the lower mantle. Geophys. Res. Lett. 40**,** 4570–4573.

van der Hilst, R.D., Widiyantoro, S., Engdahl, E.R., 1997. Evidence for deep mantle circulation from global tomography. Nature 386, 578-584.

Vinnik, L., Farra, V., 2007. Low velocity atop the 410-km discontinuity and mantle plumes. Earth Planet. Sci. Lett. 262, 398–412.

Wallace, M.E., Green, D.H., 1988. An experimental determination of primary carbonatite magma composition. Nature 335, 343–346.

Wen, L.X., Helmberger, D.V., 1998. A two-dimensional P-SV hybrid method and its application to modeling localized structures near the core-mantle boundary. Journal of Geophysical Research – Solid Earth 103, 17901-17918.

Williams, Q., Garnero, E.J., 1996. Seismic evidence for partial melt at the base of earth's mantle. Science 273 (5281), 1528-1530.

Wyllie, P.J., Ryabchikov, I.D., 2000. Volatile components, magmas, and critical fluids in upwelling mantle. J. Petrology 41 (7) 1195-1206, doi: 10.1093/petrology/41.7.1195.

Wysession, M.E., 1996. Large-scale structure at the core-mantle boundary from diffracted waves. Nature 382, 244-248.

Yoder, H.S., Tilley, C.E., 1962. Origin of basalt magmas: an experimental study of natural and synthetic rock systems. J. Petrology, 3, 342–532.

Yu, S., Garnero, E.J., 2017. A global assessment of ultra-low velocity zones, Geochem. Geophys. Geosys., to be submitted.

Zerr, A., Diegeler, A., Boehler, R. 1998. Solidus of Earth's deep mantle. Science 281, 243-246.

Zhou, Y.H., Miller, G.H., 1997. Constraints from molecular dynamics on the liquidus and solidus of the lower mantle. Geochim. Cosmochim. Acta 61 (14), 2957–2976.

Figure captions

Figure 4.1. Global distribution of ULVZ based on seismic studies from Shule and Garnero (2017), summarizing all seismic studies to date. LLSVPs (in pink) are defined by 30% of the CMB's area occupied by the lowest shear wave velocity dVs from the S40RTS tomography model (Ritsema et al., 2011). In light blue are plotted the highest velocities in the model, and 30% of the area of the CMB with those highest dVs. Red dots or patches represent regions where authors say there is a ULVZ. Blue dots or spots are regions where authors say they did not see evidence for a ULVZ. Note: a "non detection" does not rule out the possibility of a super thin ULVZ, typically < 5 km.

Figure 4.2. Reproduced from Stixrude et al. [2009]. Predicted melting curve of $MgSiO_3$ bridgmanite (red line with shaded uncertainty envelope) compared with a modern mantle geotherm (blue thick line) and a lower thermal boundary layer that reaches a temperature of 4100 K at the core–mantle boundary (Nimmo et al., 2004; Steinle-Neumann et al., 2001). Blue thin line : geotherm of Brown and Shankland (1981). The mantle solidus (thick black line) is estimated from the calculated melting curve of $MgSiO_3$ brigdmanite corrected with a freezing point depression which is assumed to vary linearly with pressure from the experimental value at 25 GPa (340 K) (Tronnes and Frost, 2002) to 1300 K at 136 GPa (Zhou and Miller, 1997). Experimentally based estimates of the mantle solidus including upper bounds on the peridotite solidus are shown (symbol: (Holland and Ahrens, 1997); thin black line: (Zerr et al., 1998)), and the basalt solidus (thin green line: (Hirose et al., 1999)). Dashed lines represent extrapolation of measurements to the CMB.

Figure 4.3. Reproduced from Gomi et al. [2013]. Liquid isentrope with minimum CMB temperature at 4.5 Gy (de Koker and Stixrude, 2009) compared with melting domains of chondrite (red, Andrault et al., 2011), peridotite (green, Fiquet et al., 2010; yellow, Stixrude et al., 2009), and Mg_2SiO_4 (blue, Mosenfelder et al., 2007).

Figure 4.4. X-ray diffraction 2D image and integrated pattern recorded for a typical peridotitic sample at 90 GPa after heating at 2800 K. The interpretation of integrated X-ray diffraction pattern shows with no ambiguity 3 co-existing phases: bridgmanite (black ticks), Ca-perovskite (blue ticks) and ferropericlase (red ticks).

Figure 4.5. Stable mineral phases assemblage of MORB at 58 GPa after heating at sub-solidus conditions (T = 2600 K). The diffraction pattern is background subtracted. All peaks can be assigned to the following phases: Mg-Pv (MgPV) or bridgmanite, Ca-Pv (CaPv), SiO_2 (St) and Ca-ferrite-type (CF) phase. Adapted from Pradhan et al. (2015).

Figure 4.6. Solidus temperature (solid circles) of MORB from Pradhan et al. [2015] plotted along with solidus for MORB from multi-anvil work (Hirose and Fei, 2002) and LH-DAC (Andrault et al., 2014; Hirose et al., 1999). The solid line (red) is a fit using the Simon–Glatzel model (Simon and Glatzel, 1929). Mantle geotherms (dashed line) is estimated from

bridgmanite to post-perovskite transition (Oganov and Ono, 2004). Adapted from Pradhan et al. (2015).

Figure 4.7 A. Modified from Andrault et al. (2016). Present-day temperature profile in the Earth's (a) mantle and (b) core inferred from several experimental arguments. Green circle corresponds to the most likely temperature at the core–mantle boundary. (a) At the CMB, melting temperatures of 4180, 4150, 3800 and 3570K were reported for peridotite (F-10, Fiquet et al. 2010), chondritic-type mantle (A-14, Andrault et al. 2014), mid-ocean ridge basalt (A-11, Andrault et al. 2011 and P-15, Pradhan et al. 2015) and wet-pyrolite (N-14, Nomura et al. 2014), respectively. Dashed curves stand for adiabatic profiles (M-07, Matas et al. 2007; H-05, Hernlund et al. 2005; K-10, Katsura et al. 2010; BS-81, Brown and Shankland, 1981; B-01, Bunge et al., 2001).

Figure 4.7 B. Adapted from Andrault et al. (2016). Melting of pure Fe was reported at 4175 and 6230K for pressure conditions of CMB (135 GPa) and ICB (330GPa), respectively (A-13, Anzellini et al., 2013). A melting temperature depression of 650K is due to the presence of light elements in the core (e.g. Morard et al., 2014). The CMB temperature is extrapolated from the ICB based on the adiabatic profile in the outer core.

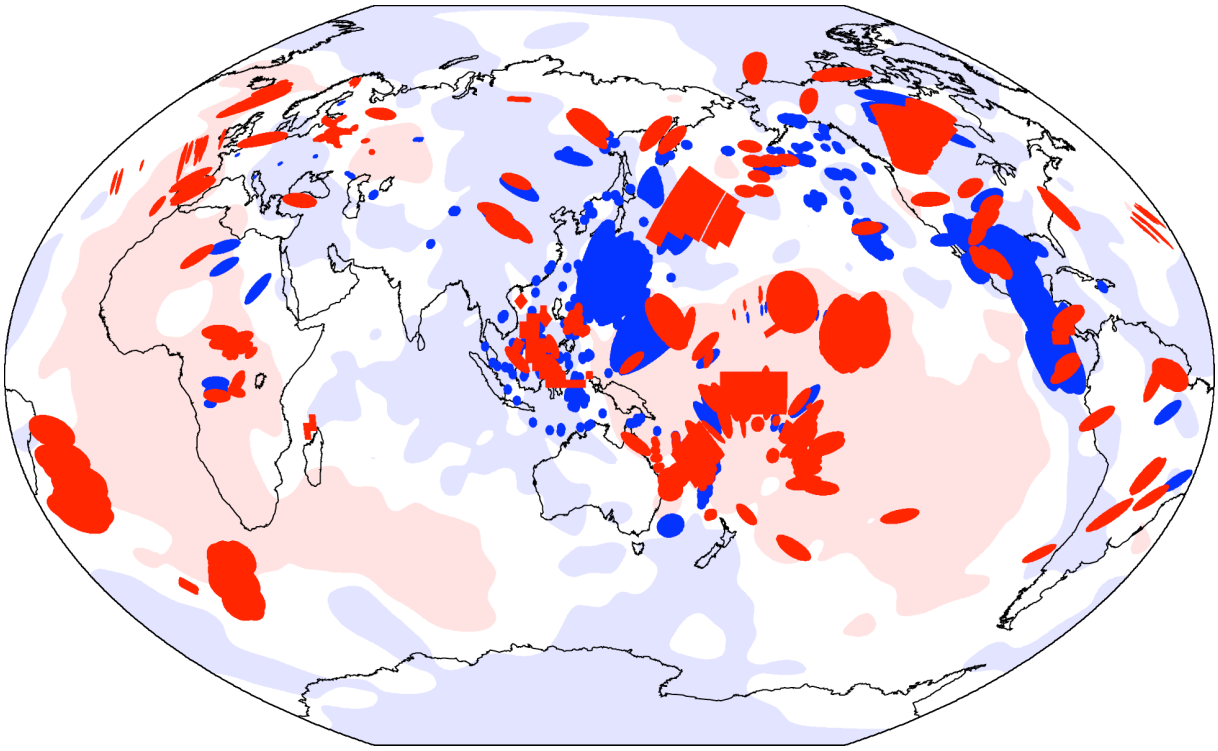

FIGURE 4.1

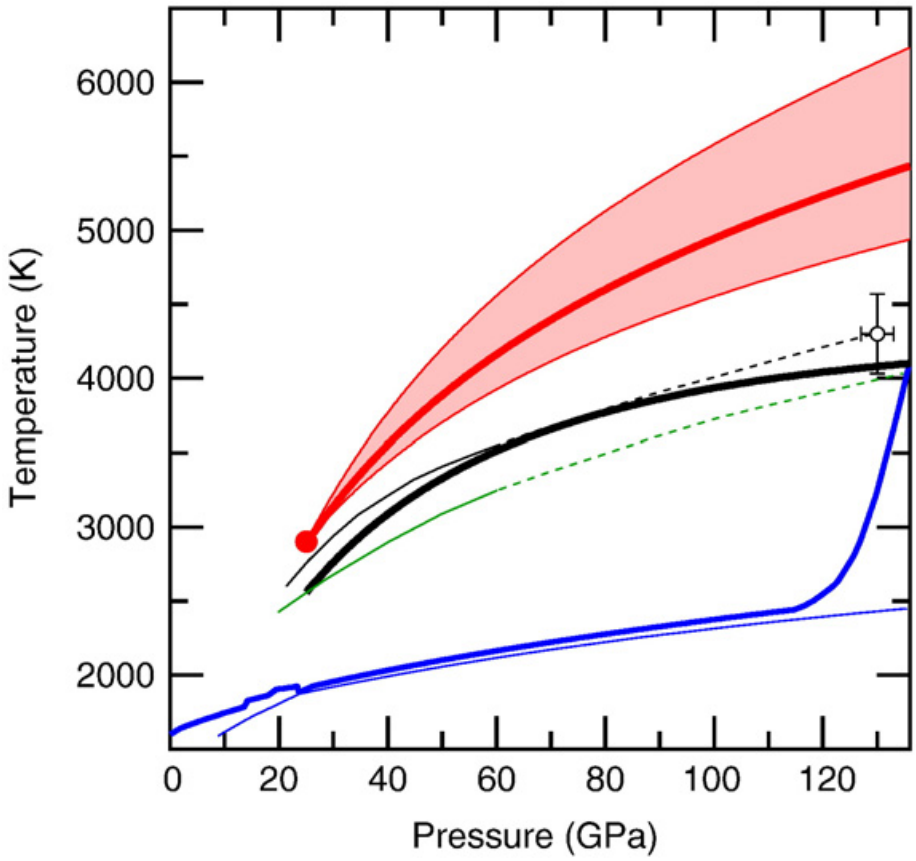
Temperature (K)
6000
5000
4000
3000
2000
0
20
40
60
80
100
120
Pressure (GPa)

FIGURE 4.2

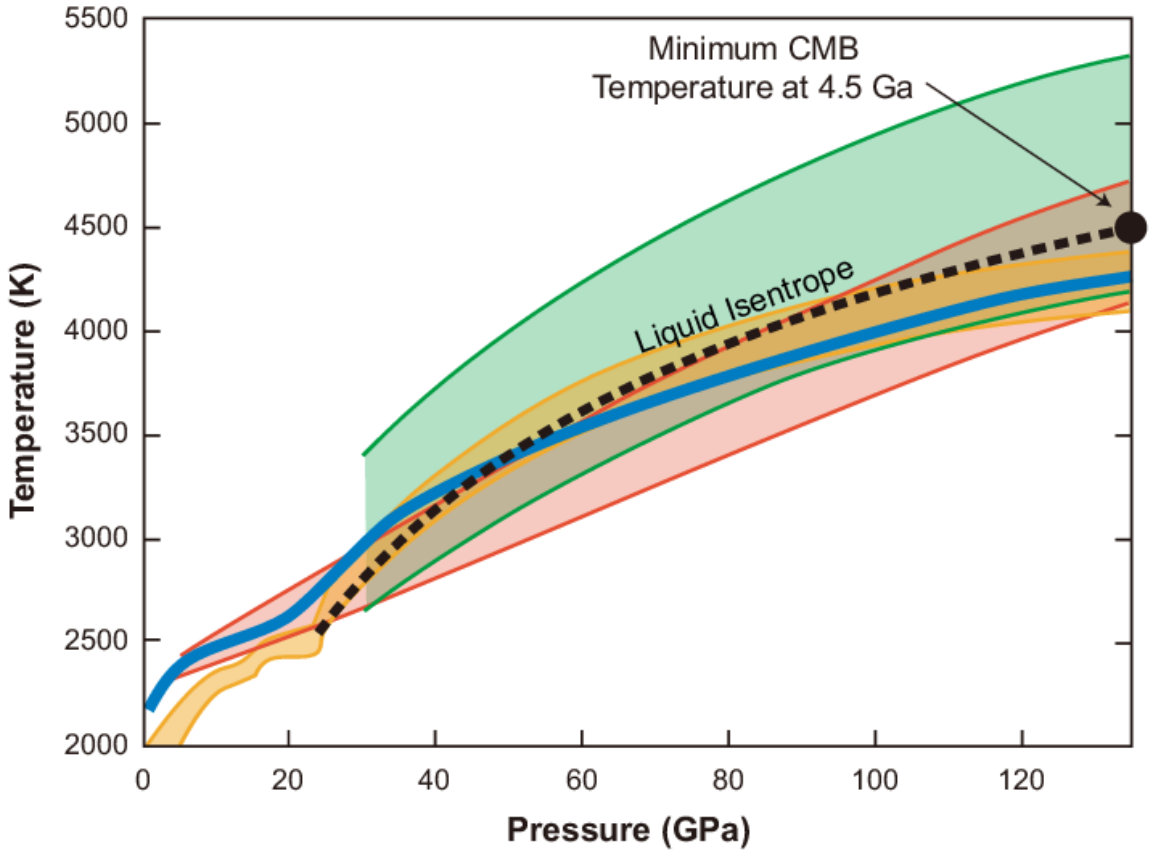
Minimum CMB
Temperature at 4.5 Ga
Liquid Isentrope
Temperature (K)
Pressure (GPa)
5500
5000
4500
4000
3500
3000
2500
2000
0
20
40
60
80
100
120

FIGURE 4.3

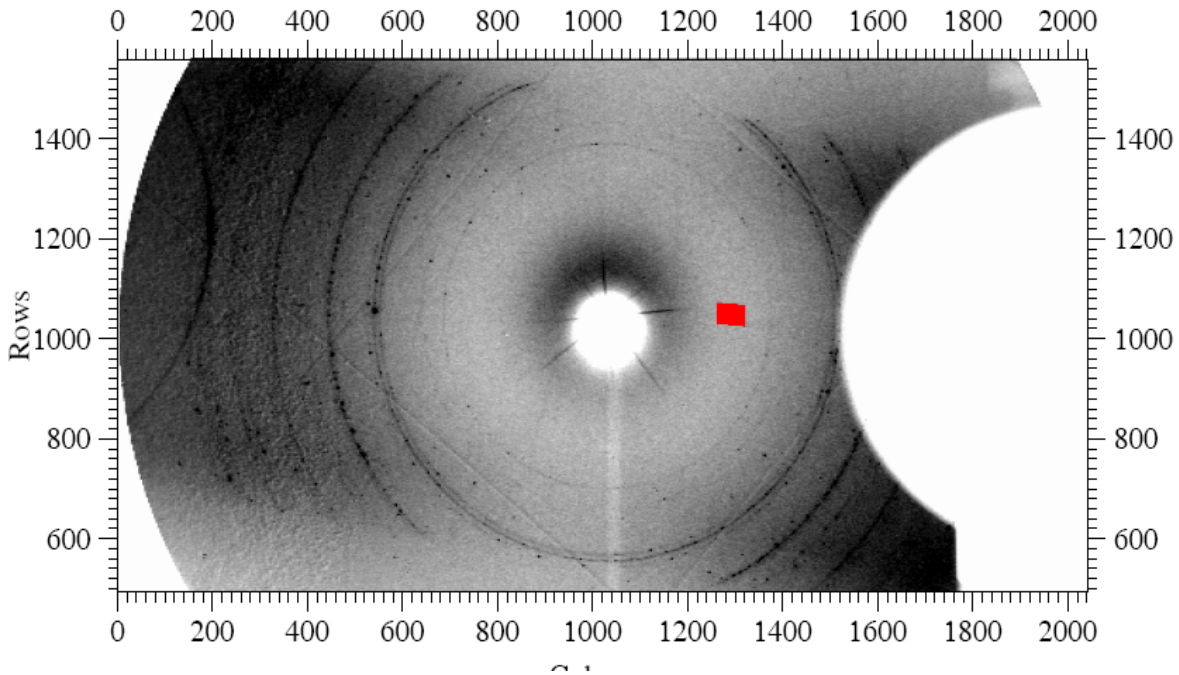
0
200
400
600
800
1000
1200
1400
1600
1800
2000
Rows

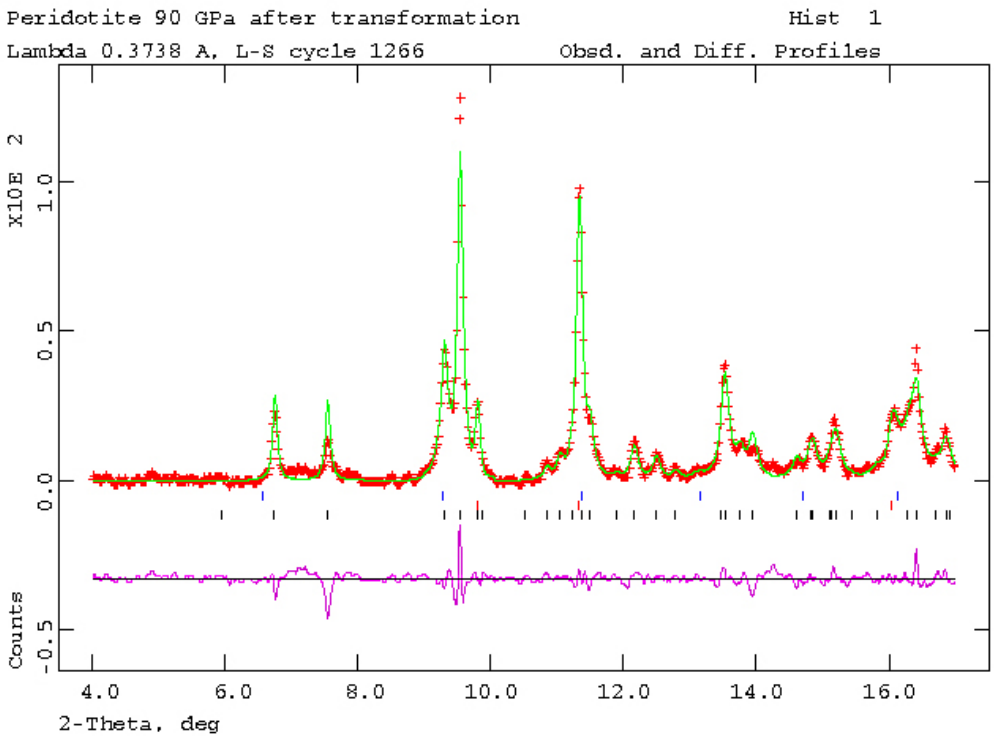
Peridotite 90 GPa after transformation
Hist 1
Lambda 0.3738 A, L-S cycle 1266
Obsd. and Diff. Profiles
X10E 2
1.0
0.5
0.0
-0.5
Counts
4.0
6.0
8.0
10.0
12.0
14.0
16.0
2-Theta, deg

FIGURE 4.4

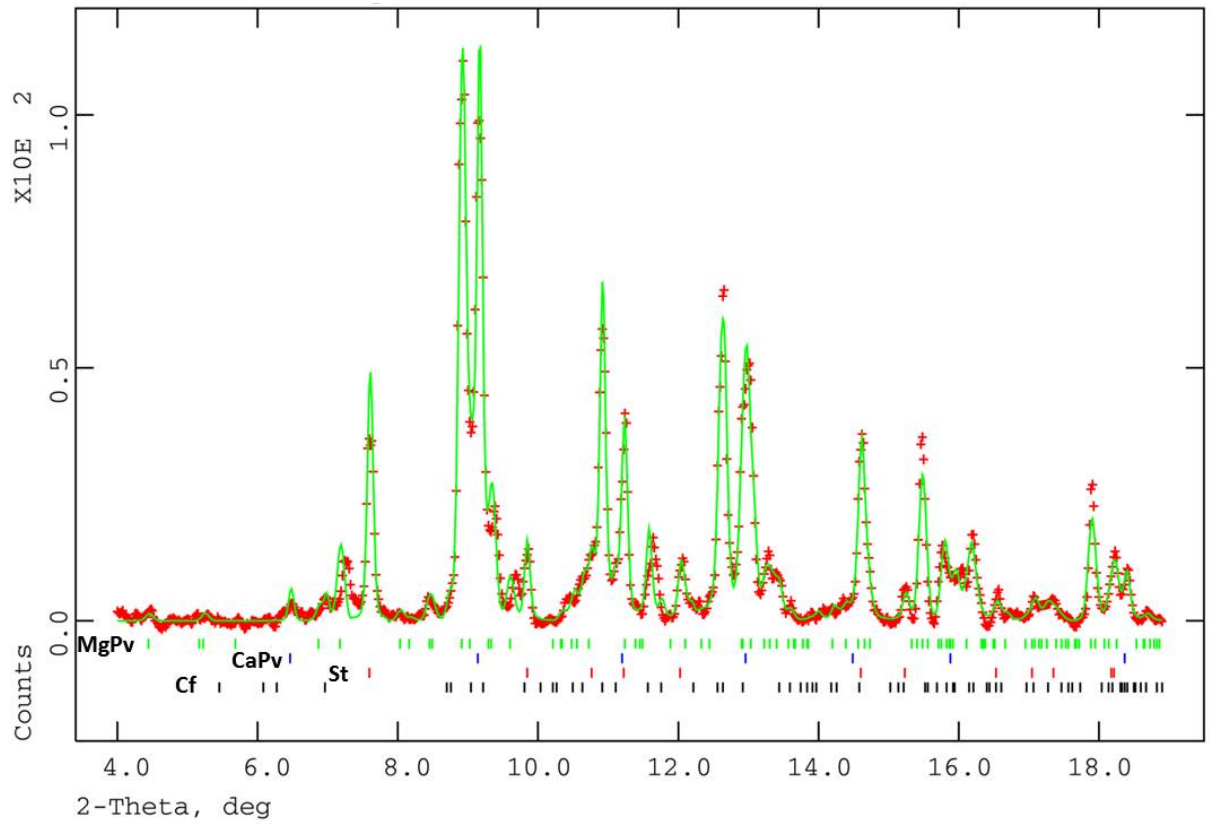
X10E 2
1.0
0.5
0.0
Counts
MgPv
CaPv
Cf
St
4.0
6.0
8.0
10.0
12.0
14.0
16.0
18.0
2-Theta, deg

FIGURE 4.5

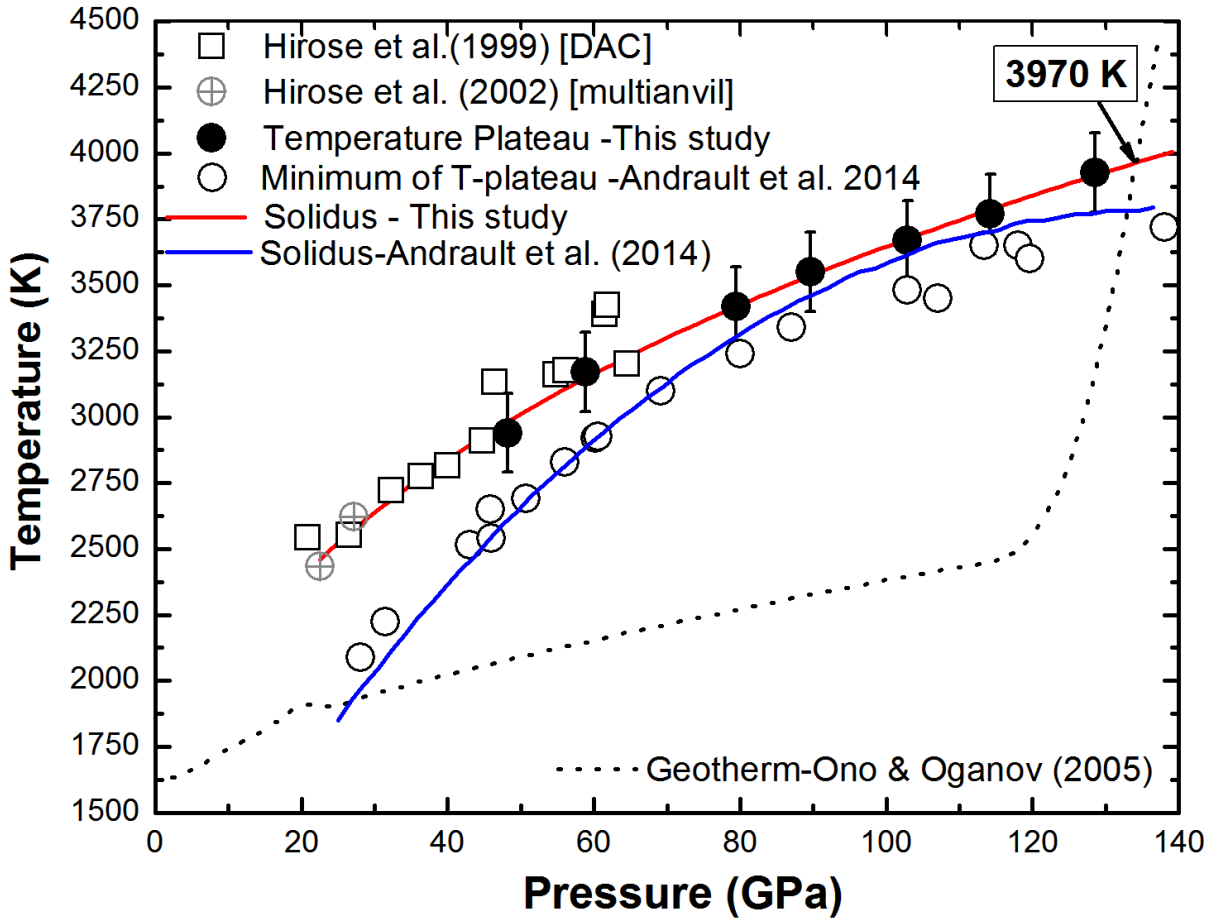
Hirose et al.(1999) [DAC]
Hirose et al. (2002) [multianvil]
Temperature Plateau -This study
Minimum of T-plateau -Andrault et al. 2014
Solidus - This study
Solidus-Andrault et al. (2014)
3970 K
Geotherm-Ono & Oganov (2005)
Temperature (K)
Pressure (GPa)
4500
4250
4000
3750
3500
3250
3000
2750
2500
2250
2000
1750
1500
0
20
40
60
80
100
120
140

FIGURE 4.6

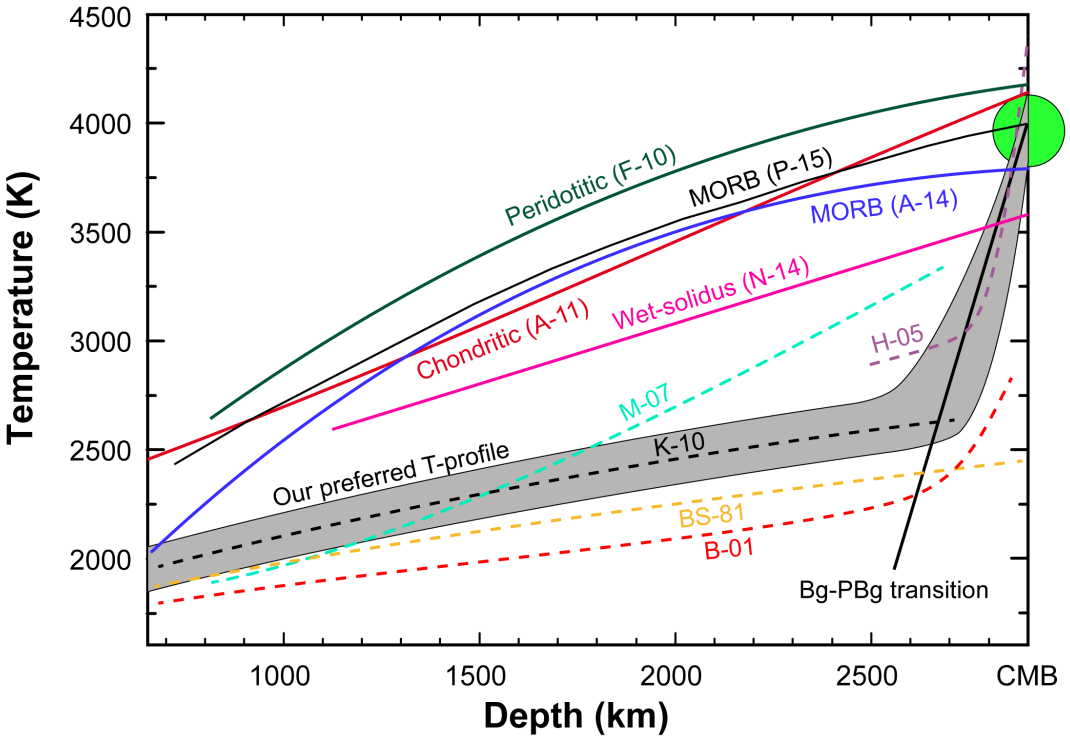
Temperature (K)
4500
4000
3500
3000
2500
2000
1000
1500
2000
2500
CMB
Depth (km)
Peridotitic (F-10)
MORB (P-15)
MORB (A-14)
Wet-solidus (N-14)
Chondritic (A-11)
H-05
M-07
Our preferred T-profile
K-10
BS-81
B-01
Bg-PBg transition

FIGURE 4.7 A

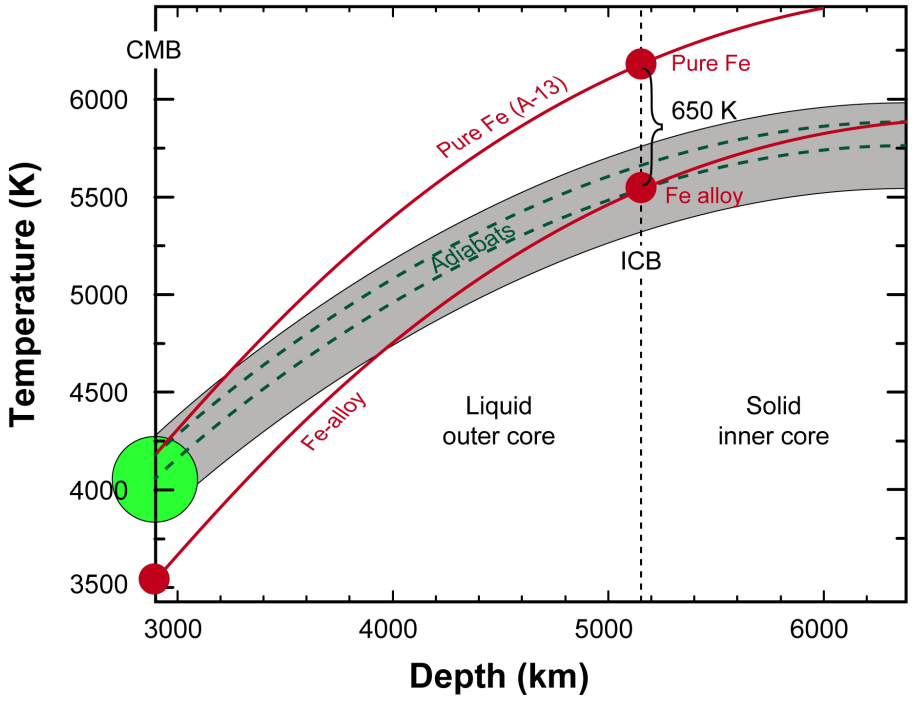
CMB
Pure Fe
Pure Fe (A-13)
650 K
Fe alloy
Adiabats
ICB
Fe-alloy
Liquid
outer core
Solid
inner core
Temperature (K)
6000
5500
5000
4500
4000
3500
3000
4000
5000
6000
Depth (km)

FIGURE 4.7 B